

PCCP

Accepted Manuscript



This is an *Accepted Manuscript*, which has been through the Royal Society of Chemistry peer review process and has been accepted for publication.

Accepted Manuscripts are published online shortly after acceptance, before technical editing, formatting and proof reading. Using this free service, authors can make their results available to the community, in citable form, before we publish the edited article. We will replace this *Accepted Manuscript* with the edited and formatted *Advance Article* as soon as it is available.

You can find more information about *Accepted Manuscripts* in the [Information for Authors](#).

Please note that technical editing may introduce minor changes to the text and/or graphics, which may alter content. The journal's standard [Terms & Conditions](#) and the [Ethical guidelines](#) still apply. In no event shall the Royal Society of Chemistry be held responsible for any errors or omissions in this *Accepted Manuscript* or any consequences arising from the use of any information it contains.

ARTICLE

Toward Hyperuniform Disordered Plasmonic Nanostructures for Reproducible Surface-Enhanced Raman Spectroscopy

Cite this: DOI: 10.1039/x0xx00000x

Received 00th January 2012,
Accepted 00th January 2012

DOI: 10.1039/x0xx00000x

www.rsc.org/C. De Rosa^a, F. Auriemma^a, C. Diletto^a, R. Di Girolamo^a, A. Malafronte^a,
P. Morvillo^b, G. Zito^c,* G. Rusciano^c, G. Pesce^c, and A. Sasso^c

We report on the self-assembling of clusters of gold-nanoparticles (Au-NPs) directed by the phase separation of poly(styrene)-*b*-poly(methylmethacrylate) (PS-*b*-PMMA) block-copolymer (BCP) on indium tin oxide coated glass, which induces the onset of vertical lamellar domains. After thermal evaporation of gold on BCP, Au-NPs of 4 nm are selectively included into PS-nanodomains by thermal annealing, and then clustered with large density of hot spots ($> 10^4/\mu\text{m}^2$) in a random two-dimensional pattern. The resulting nanostructure exhibits near-hyperuniform long-range correlations. The consequent large degree of homogeneity of this isotropic plasmonic pattern gives rise to a highly reproducible Surface-Enhanced Raman Scattering (SERS) enhancement factor over centimeter scale (std. dev. $\sim 10\%$ over 0.25 cm^2). We also discuss the application of a static electric field for modulating the BCP host morphology. The electric field induces an alignment of Au-NPs clusters into ordered linear chains, exhibiting a stronger SERS activity, but reduced SERS spatial reproducibility.

Introduction

Surface-enhanced Raman Scattering (SERS) spectroscopy allows ultrasensitive, label-free detection of the vibrational fingerprint of molecules.¹⁻⁵ This technique exploits the scattering enhancement induced when probe molecules are adsorbed onto nanostructured metal surfaces (typically Ag and Au).² On sub-wavelength nanostructures - typically formed by strongly interacting nanoparticles (NPs)⁵ - the local optical field enhancement eventually results into an effective amplification of the Raman yield up to 8 - 12 orders of magnitude.^{5,6} Fractal aggregates are among the most efficient scattering enhancers because the formation of clusters with favorable geometries induces strong cascade amplification into gap hot-spots.⁵⁻¹⁰ According to this, films of metallic nanoparticles deposited from colloidal suspensions¹¹ represent a good low-cost technology for

Electronic Supplementary Information (ESI) available: Additional methods and materials; details of the micro-Raman set-up; Raman assignment section. See DOI: 10.1039/b000000x/

ultrasensitive spectroscopy^{2,5} and biochemical sensing,¹²⁻¹⁴ but pay the cost of low reproducibility due to their intrinsically disordered morphology. Therefore engineering of SERS-active substrates is crucial in order to achieve uniform, large and reproducible substrate enhancement factors EF .¹⁵⁻¹⁸ Significant results have been obtained in this direction by engineered substrates based on bottom-up block-copolymer (BCP) templates of nanoparticles,¹⁹⁻²² lithography-patterned templates^{23,24} and hybrid fabrication techniques.^{25,26} Among these, BCP-based fabrication can take advantage of long-range self-assembling of nanodomains into ultra-high dense arrays,²⁷ enabling dense hot-spots formation on large area. Of course, phase-separated BCP domains form regular nanopatterns (spheres, cylinders or lamellae)^{28,29} that host the metal NPs (typically, after oligomer chain functionalization).³⁰ While several efforts have been dedicated to improve large area pattern's order - as for instance, by graphoepitaxial assembly²⁹ - little attention has been paid to study disordered BCP nanostructures since disorder is usually not reproducible. However, morphologically isotropic disordered materials possessing long-range spatial correlations have revealed the possibility to expand the engineering potential in photonics by

^a Dipartimento di Scienze Chimiche, Università di Napoli Federico II Complesso Monte S. Angelo, Via Cintia 80126, Napoli, Italy.

^b ENEA Italian National Agency for New Technologies, Energy and Sustainable Development, UTP-NANO, Piazzale E. Fermi 1, 80055, Portici, Italy.

^c Dipartimento di Fisica, Università di Napoli Federico II- Complesso Monte S. Angelo, Via Cintia 80126, Napoli, Italy.

*E-mail: zito@fisica.unina.it

taking advantage of a 'designer disorder' that can be quantified by so-called hyperuniformity metrics.³¹⁻³³

In this study, we move a first step toward designer disordered plasmonic nanostructures. We propose near-hyperuniform disordered gold nanostructures, based on BCP self-assembling, to fabricate isotropic and homogenous, large-area SERS substrates with highly reproducible SERS response.

Firstly, BCP interaction with the indium tin oxide (ITO) surface of a commercial borosilicate glass produces irregularly shaped BCP domains that are homogeneously distributed with near-equal areas. Then, nearly monodisperse Au-NPs are selectively included into the affine nanodomains *via* thermal annealing. Therefore, the BCP scaffold dictates the formation of a homogenous monolayer of Au-NPs characterized by close-packed random aggregates with large density of hot-spots ($> 10^4/\mu\text{m}^2$) on large area (24 mm \times 24 mm). A 'highly homogenous' disorder is evidenced by the nanocomposite's structure factor map that shows a density fluctuation vanishing at infinite wavelength, *i.e.*, characteristic of hyperuniform disorder.³¹⁻³³ Thus we achieve an isotropic nanostructure characterized by excellent long-range homogeneity. We thoroughly characterize the spatial reproducibility of the SERS response reporting a fluctuation of the SERS intensity of 10% over centimeter scale and 2.4% on areas of $100 \times 100 \mu\text{m}^2$. To the best of our knowledge, our simple approach outperforms reported Au-NP-based transparent substrates in terms of sensitivity's uniformity and enables reliable ultrasensitive analytical applications. In the concentration range explored, the characteristic SERS intensity *vs.* analyte concentration is linear and allows nano-molar resolution.

Secondly, the assistance of an electric field during thermal annealing is explored to modulate the host-morphology. This triggers the formation of linear chains of Au-NPs in which long chain coupling is responsible for an 18-fold increase of the SERS enhancement.

Results and discussion

Near-Hyperuniform Disordered BCP/Au-NPs Nanostructure

The nanostructure is obtained by means of a random but homogenous BCP host that guides the spatial distribution of guest Au-NPs clusters *via* thermal annealing. We used a polystyrene-*b*-poly(methyl methacrylate) (PS-*b*-PMMA) block copolymer with molecular masses M_n of PS and PMMA equal to 25.0 and 26.0 Kg/mol, respectively, and polydispersity index $M_w/M_n = 1.06$. The volume ratio of 0.52 between PS block and PS-*b*-PMMA copolymer was selected to obtain a phase-separation of equally sized domain with lamellar morphology.

We investigated possible routes for inducing lamellar nanodomains with vertical orientation. In general, BCP nanostructure morphology is basically the result of two mechanisms: (i) the interactions of the copolymer blocks at both air and support interfaces (wetting effect), and (ii) the ratio between film thickness and spontaneous sizes of the microphase-separated domains (commensurability effect). In control experiments, polymer films deposited either by spin-coating or drop-casting on glass substrates *without* indium thin oxide (ITO) layer, showed planar lamellar structures, *i.e.*, parallel to the surface of the supporting substrate (as extensively discussed in ref.³⁴). We aimed at guiding assemblies of Au-NPs relying on the preferential wetting of

the PS copolymer block by gold.³⁵ In fact, this is a facile method that can provide a stabilized infiltration into PS with 100% selectivity thanks to non-equilibrium processes above the polymer's glass transition temperature.³⁵ However, in the case of planar block copolymer lamellae, Au-NPs cannot be guided to produce designed patterns since there is no differential wettability pattern at the surface. Therefore, inducing a vertical orientation of BCP lamellae is a crucial step. Regardless of the deposition technique, on ITO-coated glass we obtained the desired vertical morphology thanks to the non-preferential interface interactions between ITO and the copolymer blocks PS and PMMA. In particular, thin films of PS-*b*-PMMA, 70 nm-thick, were spin coated (3000 rpm for 30 s) from a toluene solution and annealed at a temperature above the BCP glass transition temperature (150 °C) in a vacuum chamber (10^{-3} mbar) for 6 hours. The BCP scaffold was characterized by a spatially even phase-separation of PS and PMMA on the sub-wavelength scale and with invariant average characteristics on large scale. This eventually triggered the formation of random domains of close-packed Au-NPs into PS, in agreement with the guiding mechanism discussed in ref.³⁵.

The BCP films were analyzed in transmission electron microscopy (TEM) after RuO₄ staining to achieve a better contrast between PS and PMMA domains. A representative bright-field TEM micrograph (pseudo-color scale) of the BCP film is shown in Fig. 1a with related close-up on the right panel. The blue regions correspond to stained PS lamellar nanodomains, whereas dark regions to PMMA domains. The image exhibits a film structure with regular spatial segregation of copolymers corresponding to the presence of PS and PMMA lamellae oriented with vertical interfaces (perpendicular to the ITO surface). The average lamellar spacing was estimated to be ≈ 14 and ≈ 18 nm for PS and PMMA, respectively (Fig. 1a). A monolayer of gold nanoparticles was then deposited on the lamellar BCP film (Fig. 1a) by thermal evaporation of a gold filament in high vacuum³⁵ ($\approx 9 \times 10^{-5}$ mbar). In the TEM micrograph of Fig. 1b, uniformly distributed red spots indicate the formation of dispersed Au-NP clusters. A black crossover level is inserted in the color scale by custom-made code (Matlab MathWorks) to enhance the domains contrast. After thermal evaporation, the metal/BCP nanocomposite was thermally annealed in order to enhance gold's inclusion into the affine PS domains without metal surface functionalization. SEM and TEM images (see Fig. 1c-e) reveal, in fact, full selective infiltration of Au-NPs into PS domains (with selectivity of 100%) after annealing at 150 °C. The Au-NPs have a narrow size distribution with an average diameter of $4 \text{ nm} \pm 20\%$ (see Fig.S1 in the Electronic Supporting Information (ESI)) and sub-nanometer gaps (strong plasmonic coupling). The Au atoms diffuse toward the preferred PS lamellae and produce a slight enlargement of the domains. Importantly, a disordered but homogeneous close-packed clustering of Au-NPs is observed over large area thanks to the BCP homogeneous phase-separation into randomly oriented, but regularly sized, PS and PMMA nanodomains (Fig. 1c). After TEM inspection and SERS activity characterization (as discussed below), we conclude that Au-NPs are assembled into an immobilized monolayer at the top surface of the BCP host.

ARTICLE

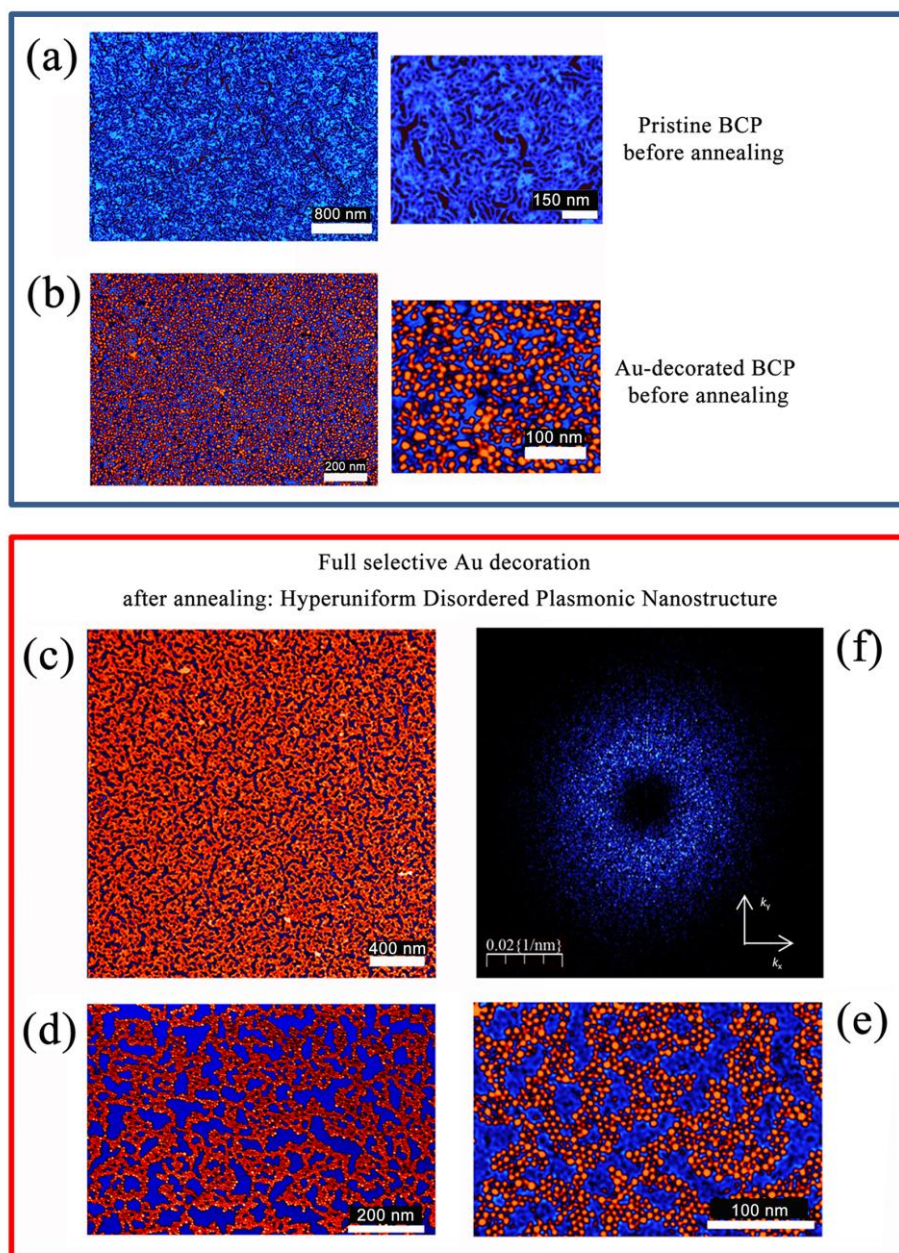


Fig. 1 a) Bright-field TEM micrograph of pristine PS-*b*-PMMA deposited on ITO supporting substrate and annealed at 150 °C for 6 hours. (b) Same as (a) after vacuum evaporation and deposition of Au-NPs forming randomly dispersed clusters (close-up on the right). (c) The post thermal annealing at 150 °C for 6 hours of the Au-BCP film in the TEM micrograph reveals the clustering in the PS nanodomains with 100% selectivity guided by the phase-segregated scaffold of the BCP. (d) Detail of the SEM micrograph of a thermally annealed Au-loaded specimen showing close-packed clustering. (e) TEM magnified scan of (c) emphasizing the selective filling of the PS domains. (f) Structure factor $S(k)$ obtained from a SEM large area micrograph revealing a spatially isotropic and invariant phase-segregation in the monolayer of Au-NPs, with near zero infinite-wavelength fluctuation (reciprocal spatial frequencies are $k_x = 1/x$ and $k_y = 1/y$ in units of nm^{-1}): the ring maximum corresponds to ~ 71.4 nm in the direct space. Scales bar are: (a) 800 nm (left) and 150 nm (right); (b) 200 nm (left) and 100 nm (right); (c) 400 nm; (d) 200 nm; (e) 100 nm.

Following the work of Torquato *et al.* about hyperuniform disorder,^{31-33,36-38} we decided to study the morphological characteristics of the random nanostructure of Fig. 1c in terms of the structure factor $S(\mathbf{k})$. According to ref.³⁷, an ideal hyperuniform

pattern is characterized by zero infinite-wavelength density fluctuations of the point pattern, *i.e.*, $S(\mathbf{k} \rightarrow 0) \approx 0$ in the reciprocal \mathbf{k} -space. In other words, given an arbitrary spherical window, the fluctuations of the point pattern grow more slowly than the window

area.^{31,32} The asymptotical behavior of this parameter can also be used to quantify the degree of homogeneity of any point pattern. Interestingly, in our case, the calculated $S(\mathbf{k}) = S(k)$ is characterized by a ring-shaped structure factor map which vanishes at $k = 0$, *i.e.*, $S(k \rightarrow 0) \approx 0$ (Fig.1f). These characteristics reveal a spatially isotropic and invariant phase-segregation with vanishing large length scale density fluctuations: a condition which points out a large degree of homogeneity despite the random nature of the clustering. Unlike crystals and quasicrystals that are trivially hyperuniform but not isotropic, disordered structures can be isotropic and hyperuniform under particular conditions. The above analysis allows us to quantify and control the actual morphological heterogeneity of the pattern of NPs. Later on, we correlate the homogeneity of these isotropic random nanostructures to a highly reproducible spatial SERS response.

Linear Chains of Au-NPs by Electric Field Assistance

In a second experiment, we explored the morphological modification induced in the pattern by electric field poling. The BCP host resulted characterized by nearly parallel and vertically oriented lamellae with long-range order. Similar morphology was reported by Amudson *et al.*³⁹ In our case, however, we applied a vertical capacitor configuration⁴⁰ for electric field poling starting from lamellae already vertically oriented (see Fig.1a), which probably facilitated the long range alignment. The electric field-assisted patterning was achieved as schematically depicted in Fig.2a. The d.c. voltage was applied for 6 hours during thermal annealing at 150 °C. ITO coated slides were used to sandwich either pristine or Au-loaded BCP films. The sample was then cooled down to room temperature while maintaining the electric field on. Bright-field TEM micrographs (pseudo-color scale) of representative samples realized under different applied electrostatic field, namely at $E_1 = 0.2 \text{ V}/\mu\text{m}$ and $E_2 = 0.32 \text{ V}/\mu\text{m}$ (cell thickness of 25 μm), are depicted in Fig.2b and 2c, respectively. The RuO₄-stained PS stripes appear colored in red. A variation of the morphology was observed as a function of increasing electric field. Firstly, the nanostructure at E_1 appeared different with respect to the uniformly disordered structure of Fig.1a (zero-field). As visible in Fig.2b, it was in fact characterized by medium-range aligned vertical lamellae of PS and PMMA with typical fingerprint morphology. Secondly, a further increase of the order degree was observed at higher field E_2 . The resulting structure was characterized by long-range, near parallel and periodic PS and PMMA nanofringes, as shown in Fig.2c. After TEM inspection at lower magnification (not shown here), the fringes appeared as characterized by a continuous length in the range of 10 μm with dislocations and declinations typical of this kind of patterned materials due to the lack of topological constraints.^{41,42} The structure factor of the aligned pattern is shown in Fig.2d: it clearly points out a one dimensional grating morphology on the micron scale. A close-up of the pattern is also shown in Fig.2e.

Following the same procedure for selective inclusion of NPs described before - this time with electric field-assisted annealing (150 °C) - the BCP pattern was characterized by periodic Au-NPs-

enriched PS stripes and Au-NPs-depleted PMMA stripes. The aligned Au-NPs chains showed sub-nanometer gaps. This is clearly evident in the TEM image of Fig.2f and the related magnifications in Fig.2g-h, which show how Au-NPs (colored in red) mainly fill the stained PS layers with a selectivity higher than 70%. The average spacing of PS lamellae is estimated to be $\approx 60 \text{ nm}$ after inclusion of gold.

SERS Enhancement Factor and Large-Area Spatial Reproducibility

A preliminary SERS characterization was conducted on several samples and control specimens using the template polymer film as analyte. This analysis was carried out to determine the blank reference spectrum of the BCP/metal nanocomposite and the related limitations regarding SERS detection imposed by the BCP presence. This also allowed us to study several gold nanostructures' characteristics. In particular, this characterization was carried on the following specimens: *A*) pristine PS-*b*-PMMA film as is; *A**) same film as *A* but after decoration with Au-NPs (as depicted in Fig. 1b); *B*) PS-*b*-PMMA film decorated with close-packed clusters of Au-NPs into uniformly disordered PS domains (as depicted in Fig. 1c-e); *C*) film of atactic polystyrene (aPS) homopolymer decorated with Au-NPs (not shown here); *D*) long-range nanofringes of PS-*b*-PMMA decorated with Au-NPs (as depicted in Fig. 2f-h). For simplicity, hereafter these samples will be referred to as *A*, *A**, *B*, *C* and *D*, respectively.

The UV-Vis extinction spectra (Perkin Elmer Lambda 35) of substrates *B* and *D* are shown in Fig.3. Remarkably, the plasmon-polariton response of *D*, centered at 578 nm, was blue-shifted with respect to the close-packed random structure *B* having an extinction peak at 594 nm. Given the large red-shift from the isolated NP (4 nm) response, it is evident that a strong plasmonic coupling due to the clustering must be taken into account to explain the observed extinction peaks. However, inferring definitive conclusions on the SERS properties of the substrates through their far field response is not trivial given the general lack of direct correspondence with the near-field response in complex clusters' structures.⁴³ Given the limited polydispersity of the observed Au-NPs ($\approx 20\%$, see Fig.S1 in ESI), we argue that plasmon hybridization in the clusters⁴⁴ can be responsible of the broad plasmonic response observed in *B*. On the other hand, the narrower extinction of *D* could result from the onset of subradiant plasmon polariton modes (dark modes).^{45,46}

It is worth mentioning that we decided to deposit small NPs in order to improve substrate's transparency, being the resulting lower scattering efficiency partially compensated by highly dense hot-spots with sub-nanometer gaps. The transmittance peak measured by UV-Vis was $\geq 80\%$ (Fig.3). Of course, the fabrication method is versatile and does exclude the possibility to decorate the BCP scaffold with larger NPs (or other materials like silver, which will be describe elsewhere).

ARTICLE

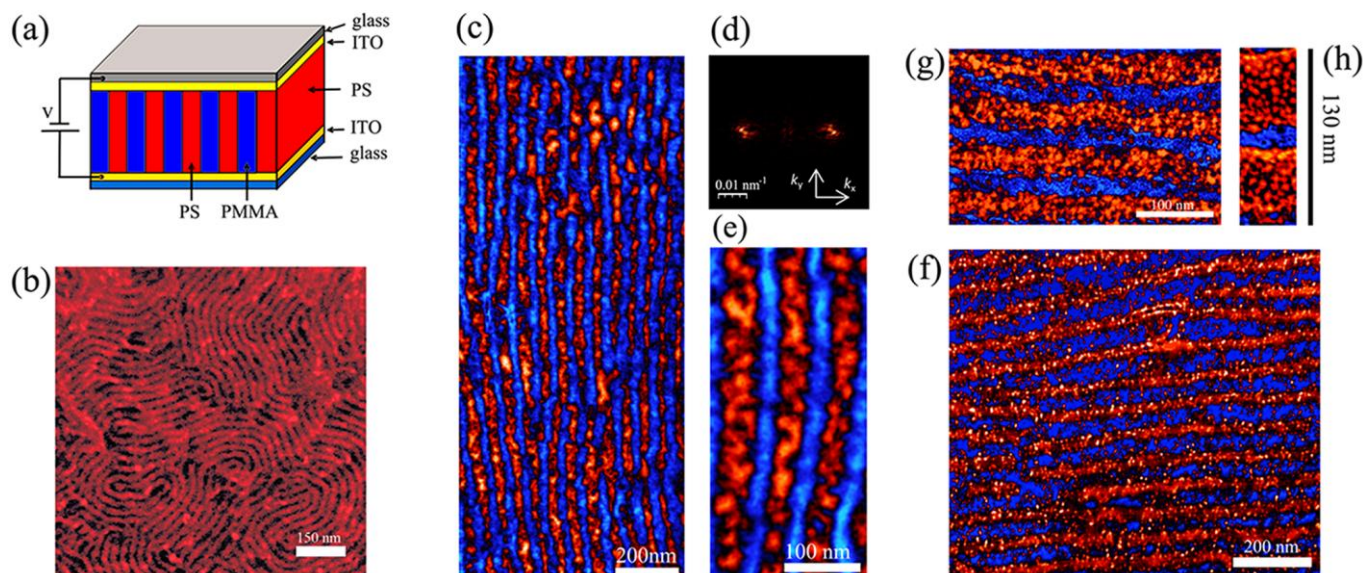


Fig. 2 (a) Schematic representation of the vertical capacitor device for electric field-assisted thermal annealing inducing vertical stacks of phase-separated BCP. (b) Bright-field TEM micrograph (false color scale) of PS-*b*-PMMA film deposited on ITO substrate and annealed at 150 °C upon electric field poling at 0.2 V/ μ m. (c) TEM scan of long-range PS stripes (red) in PMMA (blue) formed for an applied field of 110 V/ μ m during same thermal treatment. The characteristic FFT structure factor in (d) emphasizes the one-dimensional modulation along the direction perpendicular to the nanofringes of (c), with spot maximum corresponding to $1/(0.017 \text{ nm}^{-1}) = 58.8 \text{ nm}$. These last are also magnified in (e). PS is everywhere stained with RuO₄ for increasing the contrast, and a black crossover level is used in the color scale to enhance the fringes contrast with a custom-made code. (f) TEM scan (as before) for long-range nanofringes decorated with Au-NPs and annealed at 150 °C upon electric field poling at 0.32 V/ μ m. (g) TEM close-up of (f), with further magnification in (h) for resolving nanoparticles clustering.

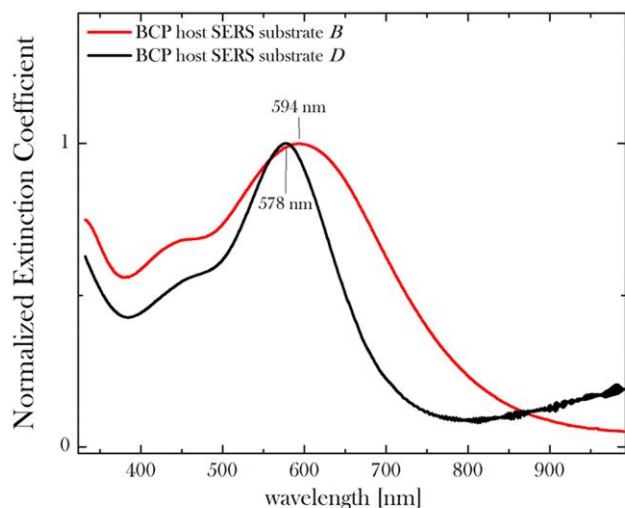


Fig. 3 Extinction spectra of the BCP nano-patterns decorated with Au-NPs for SERS substrates *B* (uniformly disordered clustering) and *D* (long-range linear chains). The plasmon resonance is found to blue-shift in the case of nanofringe morphology.

The SERS activity of the BCP/metal nanocomposites and Raman signature of the pristine BCP host were studied with a confocal micro-Raman analysis as described in the Methods and Materials

section (extended in ESI). For all Raman/SERS measurements, the excitation wavelength was 532 nm. The probed scattering area on the sample, constrained by confocal detection in backscattering collection, was accurately measured to be $A_{\text{scat}} = \pi w_o^2 = 0.44 \mu\text{m}^2$ (beam waist $w_o = 373 \text{ nm}$) by means of a knife-edge-like procedure following Cai *et al.*⁴⁷ (see ESI). Similarly, the scattering volume was estimated to be $V_{\text{scat}} = 2.0 \mu\text{m}^3$ with an effective confocal thickness of $h = 2.6 \mu\text{m}$.

Due to the reduced film thickness (70 nm) and related intrinsic low sensitivity of spontaneous Raman scattering, we used a laser power $P_{\text{in}} = 27 \text{ mW}$ for film *A* (no Au-deposition) but only of 300 μW for the polymer/gold nanocomposite films *A**, *B*, *C* and *D*. Integration time was $\Delta t = 10 \text{ s}$. For comparison, the Raman spectra of *A*, *B* and *C* are reported in Figs.4a, 4b and 4c, respectively. As shown in Fig.4a, the main spontaneous Raman bands of PS are located at 1000, 1034, 1602, 2904 and 3054 cm^{-1} , whereas the PMMA-related more intense peaks are at 812, 1450, 1734 and 2930 cm^{-1} (see ESI for peak assignment based on refs⁴⁸⁻⁵⁰). PS mainly contributed to the SERS signal with a peculiar fingerprint characterized by enhanced bands at 1155, 1200 and 1450 cm^{-1} and the emerging of a pronounced band at 1545 cm^{-1} (Fig.4b) probably due to enhanced C-H deformation⁵¹ signal associated with PS phenyl rings normally oriented to the Au-NPs surfaces. Importantly, from the comparison of Fig.4a and 4b, SERS contribution of PMMA appears negligible, which is consistent with the selectively clustering of Au-NPs into

ARTICLE

PS domains. In addition, the close-packed clustered Au-NPs of substrate *B* showed higher SERS enhancement than the smaller clusters dispersed on the aPS film of substrate *C* (Fig.4c). Finally, similarly to *C*, the Au-decorated specimen *A** gave a weak blank SERS spectrum (not shown here) of the copolymer mainly ascribable to PS as well. The blank SERS spectrum of the specimen *D* (not shown here) did not manifest any significant variation with respect to substrate *B*. The bottom line is that the large close-packing in *B* and *D* (guided by the copolymer processing) gave rise to higher SERS enhancements. A qualitative amplification of the Raman yield of the polymer host in *B* was estimated to be $\approx 10^3 - 10^4$ from the direct ratio between the intensities of the bands of PS measured on sample *A* and substrate *B*.

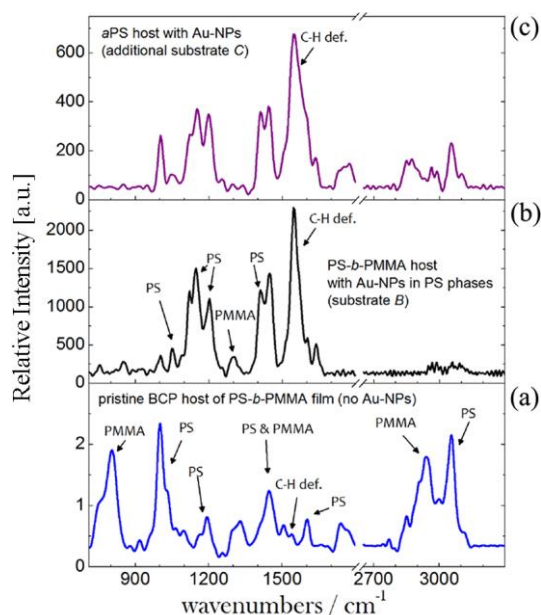


Fig. 4 (a) Raman spectrum of specimen *A*: pristine film (before gold-decoration) of PS-*b*-PMMA. (b) Raman spectrum of blank SERS substrate *B* pointing out mainly the PS signature amplified by the plasmon resonance. (c) SERS activity of a film of pure atactic homopolymer of polystyrene (aPS) decorated with Au-NPs, i.e. substrate *C*. The Raman intensity was normalized for comparison to the excitation laser power: 27 mW for (a); 300 μ W for (b) and (c).

However, a proper estimation of the SERS enhancement factor requires quantifying the number of molecules involved in the effective range of amplification of the metal surfaces.

To this end, the substrate enhancement factors EF (as defined in ref. ⁸) were estimated by using a monolayer of tris(4-(dimethylamino)phenyl) methylum chloride (crystal violet, CV, from Sigma Aldrich) that was uniformly deposited on the substrates by means of a water evaporation-based procedure (see ESI). This allowed achieving a good uniformity of the CV spatial distribution, which was inherently confirmed by the spatial uniformity of the experimentally measured SERS intensity. This method allowed us

quantifying the number of molecules in A_{scat} and estimating the average SERS EF and its spatial reproducibility over large area. This last was characterized by infiltrating 100 μ l of 380 nM CV water solution in a micro-chamber formed by two equal substrates, each having a surface of $24 \times 24 \text{ mm}^2$. Following water evaporation, the average number of molecules left adsorbed to the surface in the laser scattering area ($A_{\text{scat}} = 0.44 \text{ }\mu\text{m}^2$) was estimated to be $\approx 8.5 \times 10^3$. TEM inspection confirmed an unvaried structure with immobilized nanoparticles after water evaporation. By translating the sample with a piezo nano-positioner (see Materials and Methods and ESI), multiple sampling positions (size given by the laser spot) were probed within large raster scan areas, either of $40 \times 40 \text{ }\mu\text{m}^2$ or $100 \times 100 \text{ }\mu\text{m}^2$. In particular, a representative CV SERS spectrum measured on substrate *B* is shown in Fig.5a. The spectrum is averaged over an area of $100 \times 100 \text{ }\mu\text{m}^2$ ($P_{\text{in}} = 50 \text{ }\mu\text{W}$, $\Delta t = 10 \text{ s}$) from a statistical ensemble of 100 detection spots. The fluctuation of the SERS signal acquired over the scansion area is found to follow the normal distribution (typical of very uniform substrates⁵²) with a relative standard deviation of the total intensity $\sigma_{\text{T}} = 3.9\%$ (no background subtraction) and a relative standard deviation of the Raman amplitude $\sigma_{\text{R}} = 2.4\%$ (background subtracted). This is shown in Fig.5b, in which the normal probability plots of both ensembles are reported. A wider range was also probed by averaging the spectra acquired in 400 positions selected from 5 areas of $40 \times 40 \text{ }\mu\text{m}^2$, within an overall window of $0.5 \times 0.5 \text{ cm}^2$. This analysis revealed a Gaussian fluctuation characterized by a relative standard deviation $\sigma = 10\%$, as depicted in Fig.5c, despite the *centimeter scale* translation.

The total average SERS enhancement factor of substrate *B* was estimated to be $EF_{\text{B}} = 1.16 \times 10^6 \pm 10\%$ from the straightforward calculation given in ESI. It is our opinion that such an ultra-high reproducibility of the EF_{B} is due to the spatially regular phase-separation of PS and PMMA domains and consequent segregation with near-hyperuniform long range correlations of the close-packed Au-NPs (Fig.1f). In fact, although these nanodomains are randomly aligned, they are consistently self-repeating on large area and composed by nearly monodisperse Au-NPs producing a large density of hot-spots, i.e., $\sim 2 \times 10^4/\text{ }\mu\text{m}^2$. At each position, the laser averages the response of many gain-equivalent clusters - even within a small beam waist ($w_0 = 373 \text{ nm}$) - and leads to an enhanced signal largely uniform and reproducible because of the large density of NPs achieved with this approach.

The same spatial characterization carried out for *B* was also carried out for substrate *D* (Fig.2f). We compared the SERS spectra of CV measured on substrates *B* and *D* under equal experimental conditions of CV distribution and Raman excitation/collection as shown in Fig.5d. A significant further amplification of the Raman yield, namely ≈ 18 -fold more than substrate *B*, was measured on the

ARTICLE

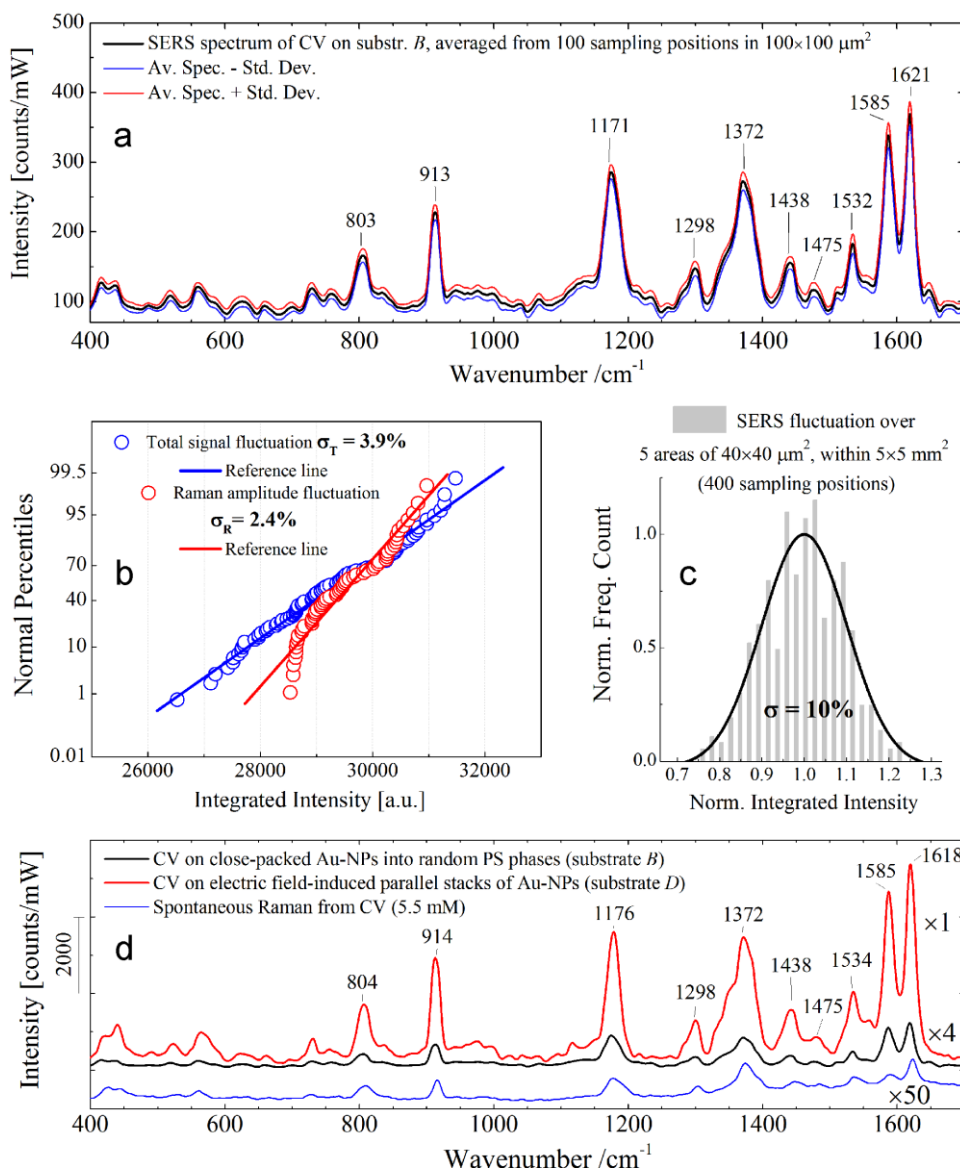


Fig. 5 (a) SERS average spectrum of Crystal Violet (CV) on substrate *B* (black curve) with related hyperspectral fluctuations (red and blue curve) over $10^4 \mu\text{m}^2$. (b) Normal probability plot of the SERS total (blue) and Raman amplitude (red) integral intensities as acquired in (a) averaged on the six more intense bands of CV at 808, 914, 1175, 1370, 1585 and 1620 cm^{-1} (see also Raman assignment of CV in Table.S1, ESI). (c) Statistical distribution of large area (0.25 cm^2) fluctuation of SERS integral intensity of CV on substrate *B*. (d) Comparison between SERS spectra of CV from substrate *B* (black) and substrate *D* (red) under identical experimental conditions for comparison of morphology dependent-enhancement. After comparison with the spontaneous Raman signal measured from bulk CV (5.5 mM) (blue line), it is evident that there is no BCP signal hindering SERS detection of CV. PS peaks are not visible because of the lower Raman differential cross section of PS with respect to CV, a Raman pre-resonant molecule.⁵⁴

ordered PS-*b*-PMMA/Au film *D*.

Therefore, for substrate *D*, a spatially average enhancement of $EF_D = 2.1 \times 10^7$ is straightforwardly estimated. A better tuning of the coupled-plasmon resonances of the NPs chains¹⁰ (see Fig.3) or a stronger coupling⁴³ might be responsible for this effect. Substrate *D* showed a good but reduced uniformity of the enhancement factor EF_D as limited to 8.3% on smaller scale of $10 \times 10 \mu\text{m}^2$, and to 20%

on larger sampling area of $40 \times 40 \mu\text{m}^2$, as expected given the larger morphological heterogeneity of morphology *D* with respect to substrate *B* at the laser spot size scale. Finally, similar characterizations carried out on substrates *A** and *C* pointed out a reduced reproducibility with a relative standard deviation of $\sim 30\%$ over $40 \times 40 \mu\text{m}^2$ and lower average enhancements, estimated to be

$EF_A = 7.2 \times 10^4$ and $EF_C = 3.0 \times 10^4$, respectively. Of course, although NPs size distribution is equivalent, the different nanoparticles close-packing is expected to influence the response of the substrates in terms of SERS enhancement and reproducibility. After comparison of the substrates' characteristics, we conclude that SERS spatial reproducibility is highly improved in substrate *B* thanks to the homogenous clustering of Au-NPs.

Nanomolar Resolution by Linear Response of SERS Intensity

In the case of substrate *B*, given the normally distributed SERS intensity over large scale (Fig.5c), we also assessed the capability of providing a quantitative determination of the CV analyte molecule. We consecutively deposited monolayers of CV molecules by water-based evaporation (see ESI) starting from $100 \mu\text{l}$ of $\sim 3.1\text{-nM}$ dilute solution spread over $2 \times 576 \text{ mm}^2$ (the factor 2 arises from the two substrates of the cell). Then, we progressively infiltrated more concentrated quantities, in steps of ~ 10 and $\sim 25 \text{ nM}$ for the measurements at low concentration. At each step, we measured the SERS signal in a region close to the first measurement.

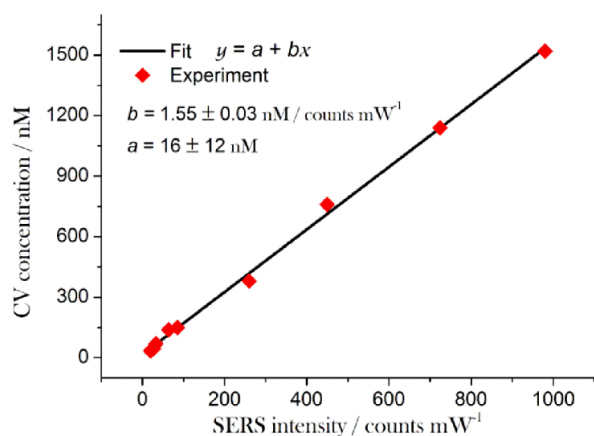


Fig. 6 Quantitative SERS measurements achievable on Au-BCP substrate *B* pointed out by independent, consecutive depositions of quantified amount of CV molecules on the same substrate and related linear response.

In Fig.6, we plot the remarkable linear trend of the SERS response measured on substrate *B*. The power was set at $50 \mu\text{W}$ for larger concentrations and at $300 \mu\text{W}$ for concentrations $< 150 \text{ nM}$. The threshold quantity detectable was $\sim 30 \text{ nM}$, corresponding to ~ 700 molecules in the scattering area. The detection sensitivity of the substrate was evaluated as a readout variation of 3 photon counts in the recorded SERS intensity ($P_{\text{in}} = 300 \mu\text{W}$), corresponding to a concentration variation of 9 nM (in the total liquid infiltrated) or equivalently ~ 60 molecules in the scattering area, therefore toward single-molecule sensitivity of a Raman resonant analyte⁵³ having differential Raman cross section comparable to CV's, that is $\sim 10^{-26} \text{ cm}^2/\text{sr}$.⁵⁴

Conclusions

In summary, we propose a block-copolymer-directed assembly of gold nanoparticles which allows fabricating near-hyperuniform disordered plasmonic nanostructures for highly reproducible SERS spectroscopy. We use the theory of hyperuniformity metrics to quantify actual homogeneity of our random nanostructure.^{31,37}

Remarkably, we find an unprecedented SERS reproducibility of the enhancement factor in correlation with this two-dimensional random BCP host ($\sigma_R = 2.4\%$ on area of $10^4 \mu\text{m}^2$; $\sigma = 10\%$ on 0.25 cm^2). In addition, electric field poling during thermal annealing modulates the host morphology by forming long range parallel fringes embedding linear chains of nanoparticles. An average enhancement factor of $\sim 10^6$ is found of the near-hyperuniform disordered structure, while an enhancement factor up to 2×10^7 is found for nanoparticles' chains. The polymer host having lower Raman activity does not affect analyte detection and allows an efficient immobilization of the Au-NPs. Therefore, we foresee the possibility to use our nanocomposite structure for reliable trace analysis and *in situ* monitoring of molecular processes.

We are currently exploring the possibility to increase the SERS enhancement factor by evaporating or including larger nanoparticles or by using low energy, oxygen plasma to induce metal coalescence. We are also testing these nanostructures for SERS scanning of cell membranes, for which large area and transparency of our substrate might offer great practical advantages such as the capability of statistical sampling of multiple cells in the same experiment, real-time monitoring under drug treatments, and backscattering acquisition in inverted microscope configuration. Finally, it is worth mentioning that our random nanoparticle network could allow studying novel hybrid random plasmonic media for studying light interaction and localization³³ with the further degree of freedom offered by a versatile soft matter host for active materials' inclusion.

Materials and Methods

The PS-*b*-PMMA copolymer was purchased from Polymer Source Inc. and used as received. The BCP sample is amorphous with glass transition temperatures equal to 108°C for PS and 126°C for PMMA. Prior BCP/toluene spin coating, ITO-coated slides were cleaned using a 20 wt% water solution of ethanolamine at 80°C in ultrasonic bath. Deposition of Au-NPs was realized using a Quorum Technologies K950X Turbo Evaporator. The copolymer film was positioned at a distance of 15 cm from a gold wire, wrapped around a tungsten filament. A voltage value above incandescence threshold of tungsten was applied for 3 s.

Pristine PS-*b*-PMMA and nanocomposite films were backed with a carbon film, floated off on water by poly(acrylic acid) backing and mounted on copper grids, then analyzed by TEM after staining with RuO_4 . Bright field images were acquired with a Philips EM 208S TEM (120 kV). SEM inspection was carried out with FEI Nova NanoSEM 650.

Raman/SERS spectra were acquired with the confocal micro-Raman system WiTec Alpha 300 at 532 nm, endowed with a spectrometer equipped with two diffraction gratings (600 and 1800 g/mm). Backscattering collection and detection were, respectively, through a $60\times$ dry Nikon objective (N.A. 0.8) and a CCD camera (Andor DV401A-BV-352) (1024×400 pixels) operating at -60°C (see Fig.S2 for the scheme). In this setup, the confocal condition is imposed by the core of the fiber delivering the signal to the spectrometer. A three-axis piezo-nanopositioner allowed precise control of the sampling translation with nanometer accuracy over $A = 100 \times 100 \mu\text{m}^2$. Further coarse translation allowed centimeter scale raster scanning (mapping and acquisition were controlled *via* computer).

CV was diluted into a milli-Q water solution at different concentrations, namely 3.1, 9.2, 25.4, 34.6, 43.9, 69.2, 138, 150, 380, 760, 1140, 1520 nM. Then, the employed solution was infiltrated into a cell constituted by two parallel substrates ($24 \times 24 \text{ mm}^2$), distanced by silica beads spacers of diameter depending on the desired cell thickness, from $4.8 \mu\text{m}$ ($\pm 4\%$) to $15.0 \mu\text{m}$ ($\pm 4\%$). For larger thicknesses, PET spacers (Mylar) were also employed.

The planar cell was sealed at two of the external borders with UV glue. With this approach, the liquid is infiltrated into a precisely controlled volume (see Fig.S3 of ESI). Water evaporation leaves a nearly perfect uniform layer of molecules (see ESI for details).

ACKNOWLEDGEMENTS

TEM measurements were carried out at C.I.S.M.E (Centro Interdipartimentale di Servizio per la Microscopia Elettronica) of the University of Napoli Federico II (UNINA). Financial supports from Italian Ministry of Education, University and Research, grants PRIN 2010-2011, PON01_01525 project MONICA and FIRB 2012-RBFR12WAPY, and in part by STAR Program - project 'LARA', from UNINA, 'Compagnia di San Paolo' and 'Istituto Banco di Napoli - Fondazione', are gratefully acknowledged.

References

- S. Nie and S. R. Emory, *Science*, 1997, **275**, 1102.
- X. M. Qian and S. M. Nie, *Chem. Soc. Rev.*, 2008, **37**, 912.
- M. Fleischmann, P. J. Hendra and A. J. McQuillan, *Chem. Phys. Lett.*, 1974, **26**, 163.
- Y. C. Liu, C. C. Yu and S. F. Sheu, *Anal. Chim. Acta*, 2006, **577**, 271.
- K. Kneipp, H. Kneipp, I. Itzkan, R. R. Dasari and M. S. Feld, *Chem. Rev.*, 1999, **99**, 2957.
- K. Li, M. I. Stockman and D. J. Bergman, *Phys. Rev. Lett.*, 2003, **91**, 227401.
- W. Li, P. H. Camargo, X. Lu and Y. Xia, *Nano Letters*, 2009, **9**, 485.
- E. C. Le Ru and P. G. Etchegoin, *Principles of Surface enhanced Raman Spectroscopy and related plasmonic effects*, Elsevier, Amsterdam, The Netherlands, 2009.
- R. Esteban, R. W. Taylor, J. J. Baumberg and J. Aizpurua, *Langmuir*, 2012, **28**, 8881.
- L. O. Herrmann, K. V. Valev, J. Aizpurua and J. J. Baumberg, *Opt. Expr.*, 2013, **21**, 32377.
- P. C. Lee and D. Meisel, *J. Phys. Chem.*, 1982, **86**, 3391.
- G. Rusciano, A. C. De Luca, G. Pesce, A. Sasso, G. Oliviero, J. Amato, N. Borbone, S. D'Errico, V. Piccialli, G. Piccialli, and L. Mayol, 2011, *Anal. Chem.*, **83**, 6849.
- R. Istatico, T. Sirec, R. Giglio, L. Baccigalupi, G. Rusciano, G. Pesce, G. Zito, A. Sasso, M. De Felice and E. Ricca *PLoS ONE*, 2013, **8**, e74949.
- G. Rusciano, G. Zito, R. Istatico, T. Sirec, E. Ricca, E. Bailo and A. Sasso, *ACS Nano*, 2014, DOI: 10.1021/nn504595k.
- A. M. Schwartzberg, C. D. Grant, A. Wolcott, C. E. Talley, T. R. Huser, R. Bogomolni and J. Z. Zhang, *J. Phys. Chem. B* 2004, **108**, 19191.
- H. Wang, C. S. Levin and N. J. Halas, *J. Am. Chem. Soc.*, 2005, **127**, 14992.
- L. A. Dick, A. D. McFarland, C. L. Haynes and R. P. Van Duyne, *J. Phys. Chem., B* 2002, **106**, 853.
- D. Lim, K. Jeon, H. M. Kim, J. Nam and Y. D. Suh, *Nat. Mater.*, 2009, **9**, 60.
- W. J. Cho, Y. Kim and J. K. Kim, *ACS Nano*, 2012, **6**, 249.
- G. Zito, A. Malafrente, A. Dochshyanov, G. Rusciano, F. Auriemma, G. Pesce, C. De Rosa and A. Sasso, in *Proceedings of SPIE Optics+Optoelectronics*, 2013, **87740B**, 1.
- P. A. Mistark, S. Park, S. E. Yalcin, D. H. Lee, O. Yavuzcetin, M. T. Tuominen, T. P. Russell, M. Achermann, *ACS Nano*, 2009, **3**, 3987.
- Y. Wang, M. Becker, L. Wang, J. Liu, R. Scholz, J. Peng, U. Gösele, S. Christiansen, D. H. Kim and M. Steinhart, *Nano Lett.*, 2009, **9**, 2384.
- A. G. Brolo, E. Arctander, R. Gordon, B. Leathem and K. L. Kavanagh, *Nano Lett.*, 2004, **4**, 2015.
- N. A. Hatab, C. Hsueh, A. L. Gaddis, S. T. Retterer, J.-H. Li, G. Eres, Z. Zhang and B. Gu, *Nano Letter.*, 2010, **10**, 4952.
- J. Theiss, P. Pavaskar, P. M. Echternach, R. E. Muller and S. B. Cronin, *Nano Lett.*, 2010, **10**, 2749.
- B. Yan, A. Thubagere, W. R. Premasiri, L. D. Ziegler, L. Negro and B. M. Reinhard, *ACS Nano*, 2009, **3**, 1190.
- M. Park, C. K. Harrison, P. M. Chaikin, R. A. Register and D. H. Adamson, *Science*, 1997, **276**, 1401.
- G. H. Fredrickson and F. S. Bates, *Annu. Rev. Phys. Chem.*, 1990, **41**, 525.
- E. Han, H. Kang, C.-C. Liu, P. F. Nealey, and P. Gopalan, *Adv. Mater.*, 2010, **22**, 4325.
- M. R. Bockstaller, R. A. Mickiewicz and E. L. Thomas, *Adv. Mater.*, 2005, **17**, 1331.
- C. E. Zachary, Y. Jiao, S. Torquato, *Phys. Rev. Lett.*, 2011, **106**, 178001.
- M. Florescu, S. Torquato and P. J. Steinhardt, *Proc. Natl. Acad. Sci. USA* 2009, **106**, 20658.
- N. Muller, J. Haberko, C. Marichy and F. Scheffold, *Adv. Opt. Mater.* 2014, **2**, 115.
- C. Diletto, P. Morvillo, R. Di Girolamo, F. Auriemma v C. De Rosa, *J. Nanosci. Nanotech.*, 2013, **13**, 5215.
- W. A. Lopes and H. M. Jaeger, *Nat.*, 2001, **414**, 735.
- S. Torquato and F. Stillinger, *Phys. Rev. E*, 2003, **68**, 041113/1.
- R. Xie et al., *Proc. Natl. Acad. Sci. USA*, 2013, **110**, 13250.
- C. E. Zachary and S. Torquato, *J. Stat. Mech.*, 2009, **12**, P12015.
- K. Amundson, E. Helfand, D. D. Davis, X. Quan, S. S. Patel and S. D. Smith, *Macromol.*, 1991, **24**, 6546.
- Y. Tsori and D. Andelman, *Macromol.* 2002, **35**, 5161.
- R. Ruiz, N. Ruiz, Y. Zhang, R. L. Sandstrom, C. T. Black, *Adv. Mater.*, 2007, **19**, 2157.
- C. Harrison, D. Adamson, Z. Cheng and J. Sebastian, *Science*, 2000, **290**, 1558.
- E. C. Le Ru, C. Galloway and P. G. Etchegoin, *Phys. Chem. Chem. Phys.*, 2006, **8**, 3083.
- N. J. Halas, S. Lal, S. Link, W. Chang, D. Natelson, J. H. Hafner and P. Nordlander, *Adv. Mater.*, 2012, **24**, 4842.
- Y. Sonnefraud, N. Verellen, H. Sobhani, V. V. Moshchalkov, P. van Dorpe, P. Nordlander and S. Vandenbosch, *ACS Nano*, 2010, **4**, 1664.
- D. Solis, B. Willingham, S. L. Nauert, L. S. Slaughter, J. Olson, P. Swanglap, A. Paul, W. Chang and S. Link, *Nano Lett.*, 2012, **12**, 1349.
- W. Cai, B. Ren, X. Li, C. She, F. Liu and X. Cai, *Surf. Sci.*, 1998, **406**, 9.
- K. J. Thomas, M. Sheeba, V. P. N. Nampoori, C. P. G. Vallabhan and P. Radhakrishnan, *J. Opt. A: Pure Appl. Opt.*, 2008, **10**, 055303.
- J. M. Zhang, D. H. Zhang and D. Y. Shen, *Macromol.*, 2002, **35**, 5140.

- 50 J. M. Zhang and D. Y. Shen, *Chi. Chem. Lett.*, 2002, **13**, 563.
- 51 J. S. Suh and M. Moskovits, *J. Am. Chem. Soc.*, 1986, **108**, 4711.
- 52 E. C. Le Ru, P. G. Etchegoin, and M. Meyer, *J. Chem. Phys.*, 2006, **125**, 204701.
- 53 E. C. Le Ru, J. Grand, I. Sow, W. R. Somerville, P. G. Etchegoin, M. Treguer-Delapierre, G. Charron, N. Felidj, G. Levi and J. Aubard, *Nano Lett.*, 2011, **11**, 5013.
- 54 S. A. Meyer, E. C. Le Ru and P. G. Etchegoin, *J. Phys. Chem. A* 2010, **114**, 5515.